JOURNAL OF NANO- AND ELECTRONIC PHYSICS
Vol. 8 No 3, 03022(4pp) (2016)

ЖУРНАЛ НАНО- ТА ЕЛЕКТРОННОЇ ФІЗИКИ
Том 8 № 3, 03022(4cc) (2016)

Electrophysical and Magnetoresistive Properties of the $Ni_{80}Fe_{20}$ Thin Film Alloy

O.V. Pylypenko, I.M. Pazukha, A.S. Ovrutskyi, L.V. Odnodvorets*

Sumy State University, 2, Rimsky Korsakov St., 40007 Sumy, Ukraine

(Received 28 June 2016; published online 03 October 2016)

In this work, the complex investigations of the crystal structure and phase state, the thermoresistive (resistivity, temperature coefficient of resistance), strain (integral and differential coefficients of longitudinal tensosensitivity in the strain interval of $\Delta\varepsilon_l = 0$-1 %) and magnetoresistive (magnetoresistance and anisotropic magnetoresistance) properties of the $Ni_{80}Fe_{20}$ thin film alloy have been carried out in the thickness range of 10-45 nm. The effect of condensation conditions and heat treatment on the mentioned properties has been analyzed.

Keywords: Permalloy, Structure and phase state, Temperature coefficient of resistance, Strain coefficient, Magnetoresistance, Coercivity.

DOI: 10.21272/jnep.8(3).03022 PACS numbers: 68.60.Dv, 68.60.Bs, 75.70.Ak

1. INTRODUCTION

Permalloy ($Ni_{80}Fe_{20}$) is a soft magnetic material which is widely used in the production of magnetic field sensors, magnetic tunnel junctions and other magnetoelectronic devices [1-3] due to high sensitivity, stability and, above all, magnetic properties. The widespread use of the permalloy in various fields of electronics and sensor technology has become possible due to the intensive study of its magnetic and magnetoresistive properties performed in the last decades [4-6]. Along with this, the tensoresistive properties of this film alloy were not thoroughly carried out. Most of the papers were devoted to the study of the mechanical properties (hardness, Young's modulus, etc.) [7], and the investigation of the tensoresistive properties of the permalloy films was limited to a concentration of 75 wt. % of Ni [8].

This work is dedicated to the complex analysis of the structural and phase state, electrophysical (resistivity, temperature coefficient of resistance (TCR) and strain coefficient (SC)) and magnetoresistive (magnetoresistance (MR) and anisotropic magnetoresistance (AMR)) properties of the $Ni_{80}Fe_{20}$ alloy films obtained by thermal evaporation method for the purpose of their further use as the components of spin-valve systems or granular nanostructures.

2. EXPERIMENTAL

The thin films of the $Ni_{80}Fe_{20}$ alloy were prepared by the method of thermal evaporation of 79 NM permalloy (79-80 wt. % of Ni, 4-5 wt. % of Mo, 15-16 wt. % of Fe) on the substrates of various types at room temperature with a rate of $\omega = 0.1$ nm/s in the installation VUP-5M ($p \sim 10^{-4}$ Pa). The chemical composition of the samples was controlled by energy dispersive analysis (REM-103), which ensures the determination accuracy of the components of ± 5 % (an example of the energy dispersive spectrum is illustrated in Fig. 1). The film thickness was defined by optical interferometry (device MII-4) with an accuracy of ± 10 %.

To perform studies of the thermoresistive properties, the samples, pre-deposited on glass ceramic substrates,

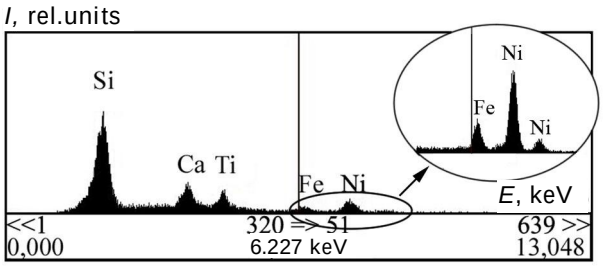

Fig. 1 – Energy dispersive spectrum for the $Ni_{80}Fe_{20}$(45)/Sub film after condensation. In brackets: the film thickness is given in nm, Sub is the substrate

were annealed for 4 "heating ↔ cooling" cycles. We note that the first cycle was limited to a defect healing temperature (it varied from 430 to 470 K depending on the sample thickness), and the next cycles were carried out in order to determine the temperature stability of the samples with increasing heat treatment cycles. The TCR value was calculated based on the temperature dependence of the resistivity for the fourth cooling cycle by the following ratio: $\beta = (1/\rho_i)\cdot(\Delta\rho/\Delta T)$, where ρ_i is the initial resistivity, $\Delta T = 5$ K.

Studies of the tensoresistive properties were carried out for condensed samples deposited on polystyrene substrates for 3 "loading ↔ unloading" cycles in the strain range of $\Delta\varepsilon_l = 0$-1 %. The calculations of the integral $(\gamma_l)_{int}$ and differential $(\gamma_l)_{dif}$ strain coefficients were performed according to the correlations $(\gamma_l)_{int} = (1/R(0))\cdot(\Delta R/\Delta\varepsilon_l)$ and $(\gamma_l)_{dif} = (1/R_i)\cdot(dR_i/d\varepsilon_{li})$, where $R(0)$ is the resistance at zero longitudinal strain; R_i and dR_i are the electrical resistance of the film samples at the beginning of the strain range $\Delta\varepsilon_{li}$ and its change with increasing longitudinal strain by $d\varepsilon_{li}$, respectively.

Studies of the magnetoresistive properties were performed by a four-point scheme in an external magnetic field from 0 to 500 mT. The current was passed parallel to the sample plane. The measurements of the MR were carried out at room temperature in three orientations of the magnetic field with respect to the current direction: perpendicular (⊥), transverse (┼) and longitudinal (∥). The value of MR was calculated in accordance with the

* larysa.odnodvorets@gmail.com

ratio $\mathrm{MR} = [(R(B)\text{-}R(B_s)/R(B_s)]\cdot 100\%$, where $R(B_s)$ is the electrical resistance in the saturation magnetic field or in the maximum possible magnetic field; $R(B)$ is the current value of the film resistance in the magnetic field. The AMR evaluation was performed by the following ratio: $\mathrm{AMR} = 3(R_\parallel - R_+)/(R_\parallel + 2R_+)$, where $R_\parallel$ and R_+ are the film resistances, respectively, with the parallel and transverse orientations of the magnetic field relative to the current direction. In order to study the influence of temperature on the magnetoresistive properties of permalloy films, the samples were kept in vacuum for 20 min at a temperature of $T_v = 470$ K, which corresponds to a defect healing temperature.

To study the phase composition and crystal structure of permalloy films before and after thermal annealing, the samples were deposited on microscopic copper mesh with a pre-applied layer of carbon. The analysis of the structural and phase state of the films was immediately carried out by electron diffraction and electron microscopy (PEM-125K).

3. RESULTS AND DISCUSSION

3.1 Structural and phase state

In Fig. 2 we illustrate the results of electron diffraction and structural studies of permalloy films in the as-deposited state and after thermal annealing at 470 K. The phase composition of the samples after condensation corresponds to the fcc-phase with the lattice parameter $a = 0.354 \pm 0.001$ nm, which is close to the parameter of Ni_3Fe intermetallic phase ($a = 0.355$ nm [9, 10]). In this case, the lines from the oxide phases are not fixed on the electron diffraction patterns that indicates a sufficiently high purity of the samples obtained after deposition.

During thermal annealing, a slight increase in the lattice parameter takes place; the phase composition remains constant and corresponds to the fcc-Ni_3Fe. Since the annealing temperature does not exceed 900 K, the formation of oxide phases does not occur during thermal treatment, as evidenced by electron diffraction analysis of the $Ni_{80}Fe_{20}$(16)/Sub film after annealing (Fig. 2b).

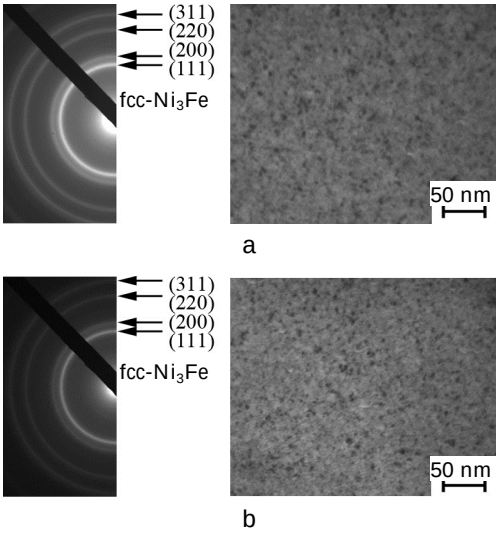

Fig. 2 – Electron diffraction patterns and micrographs of the crystal structure of $Ni_{80}Fe_{20}$(16)/Sub film after condensation (a) and thermal annealing up to 470 K (b)

As seen from Fig. 2, the film samples have a nanocrystalline structure, since the average grain size (L) does not exceed 5 nm. During thermal treatment, the sample structure remains nanosized, the value of L remains close to 5 nm that agrees with the data of [7], the authors of which obtained a similar result for the samples of permalloy $Ni_{80}Fe_{20}$ prepared by magnetron sputtering with the thickness of 50 nm. They showed that during annealing to 523 K, there is an increase in the average grain size from 4.7 to 5.3 nm, i.e. thermal treatment does not cause changes in the crystal structure of the samples.

3.2 Electrophysical properties

The temperature dependences of the resistivity and TCR typical for permalloy films are presented in Fig. 3 and have the following features. First, for the $Ni_{80}Fe_{20}$ alloy, as well as for its components in the pure form (see, for example, [11, 12]), there is a characteristic decrease in the resistivity with increasing temperature in the 1st heating cycle that is explained by the healing of defects in the crystal structure. Second, two areas with different tendencies to change resistance are observed in the dependences $\rho(T)$: in the first area, a slight increase in the value of ρ is observed with increasing T and in the second one – a sharp decrease with increasing temperature, which is completed by an insignificant increase in resistance. In this case, it should be noted that even with a slight increase in the sample thickness, there occurs an increase in the temperature range of the first area and the change in the form of the dependence of the 1st heating cycle in the second area from a relatively fast to a more flat. The reason for such changes may be the fact that with increasing sample thickness, there is a gradual increase in the temperature range, at which the healing of defects occurs. Third, the cooling curves of the 1st and all subsequent cycles are parallel to each other and even coincide in the case of the $Ni_{80}Fe_{20}$(16)/Sub sample. Such behavior is also typical for the alloy components [10, 11]. For $d = 10$-25 nm, the value of the resistivity is of the order of $\rho \sim 10^{-6}$-10^{-7} Ohm·m that is characteristic for the films of this alloy [13].

In Fig. 4 we present the temperature dependences of the TCR for the II-IV cooling cycles on the example of the $Ni_{80}Fe_{20}$(22)/Sub sample, which indicate the completion of all relaxation processes already in the 1st thermal stabilization cycle, since the TCR value is almost constant for the II-IV cycles. Moreover, the behavior of the temperature dependences of ρ (Fig. 3) and β (Fig. 4) implies a purely metallic conductivity of permalloy films or a very small contribution of the hole conductivity.

Fig. 5 illustrates the typical strain dependences in the range of $\Delta\varepsilon_l = (0 - 1)$ % for permalloy films. As seen from this figure, stabilization of the tensoresistive properties occurs starting from the II strain cycle. This is evidenced by the fact that the strain dependences in the II and III cycles are almost overlapped.

In the inset of Fig. 5 we show the dependence of the differential strain coefficient on deformation and present the value of the integral strain coefficient for the III "loading ↔ unloading" cycle. The obtained values of $(\gamma)_{int}$ correlate well with the results of [8] for the $Ni_{75}Fe_{25}$ film alloy, whose component concentration is rather close to the $Ni_{80}Fe_{20}$ alloy.

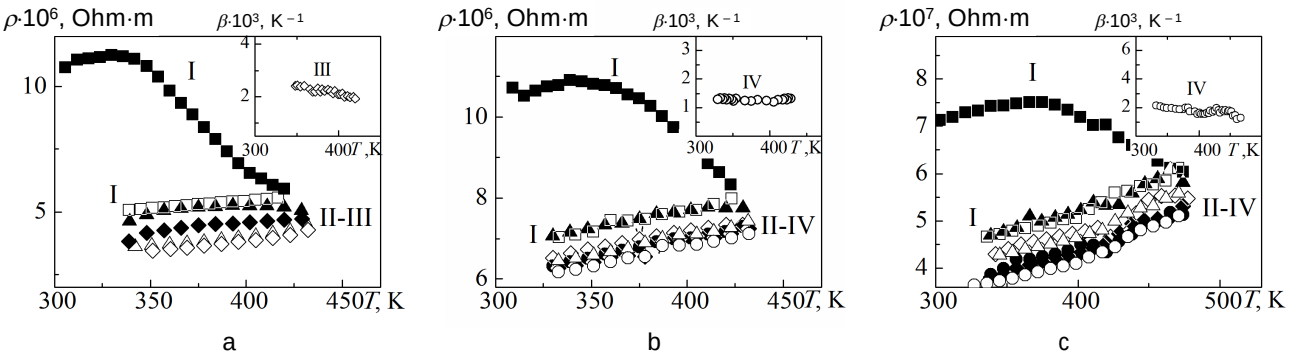

Fig. 3 – Temperature dependences of the resistivity and TCR (in the insets) for the $Ni_{80}Fe_{20}$ alloy films of the thickness of 13 (a), 16 (b) and 22 nm (c). Roman numerals denote the numbers of "heating ↔ cooling" cycles

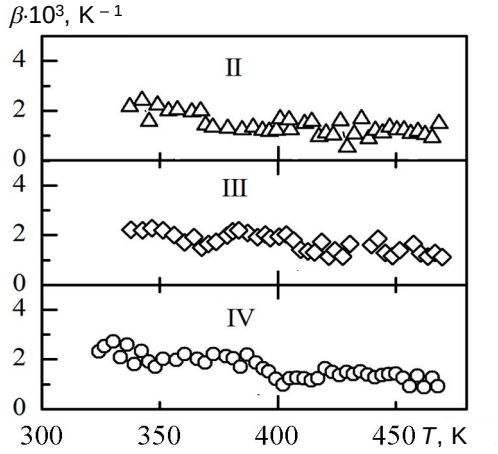

Fig. 4 – Temperature dependences of the TCR for the II-IV thermal treatment cycles of the $Ni_{80}Fe_{20}$(22 nm)/Sub film

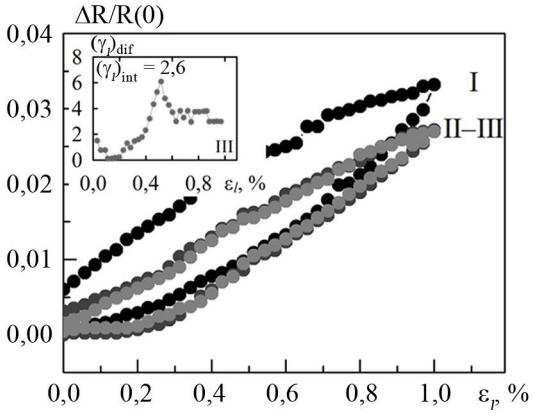

Fig. 5 – Dependences of $\Delta R/R$ and $(\gamma_l)_{dif}$ (in the inset) on ε_l for the $Ni_{80}Fe_{20}$(22 nm)/Sub film for the strain range $\Delta\varepsilon_l = (0 - 1)$ %. Roman numerals denote the numbers of strain cycles

It should be noted that with increasing sample thickness from 10 to 45 nm, there occurs an increase in the integral SC from 1.8 to 2.7. A similar increase is also typical for films with a concentration of $c_{Ni} = 75$ wt. % [8]. A tendency to increase $(\gamma_l)_{int}$, unlike the classical size dependence (SC decreases with increasing thickness [14]), is associated by the authors of [8] with the fact that studies of the tensoresistive properties were performed in the plastic range, since the transition from elastic to plastic strain occurs already at 0.2 %. The nature of the maximum in the dependence of $(\gamma_l)_{dif}$ on ε_l (see Fig. 5, the inset) has found its explanation in [15].

3.3 Magnetoresistive properties

In Fig. 6 we present the field dependence of the MR for permalloy films before and after exposure in vacuum at a temperature of 470 K for 20 min. Based on these dependences, such parameters as the saturation field, the coercive force (B_c) and the MR were determined. Among the characteristic features of the given dependences, one should highlight the anisotropic nature of the MR in the transition to the perpendicular orientation of the magnetic field with respect to the current direction and the absence of the saturation field for all three orientations of the magnetic field after condensation (Fig. 6a). The MR value at 300 K does not exceed 0.1 %. The coercive force for the transverse and longitudinal orientations of the magnetic field is close to zero, while for the perpendicular orientation, the value of B_c varies in the range from 200 to 10 mT with increasing sample thickness from 13 to 45 nm.

The process of thermal annealing leads to changes in the shape of the loops of the magnetoresistive dependences for all three orientations of the magnetic field; at that, the value of the coercive force for the transverse and longitudinal orientations is almost constant, and for the perpendicular one, as seen from Fig. 6a, b, it slightly decreases. The value of MR after annealing somewhat increases for ┼ and ∥ orientations, but insignificantly (MR < 0.1 %), while for ⊥ orientation, the MR increases almost five times. The largest value MR = 0.34 % was obtained for the sample $Ni_{80}Fe_{20}$(22)/Sub for the perpendicular orientation of the magnetic field after thermal annealing to 470 K (Fig. 6c).

Calculations of the AMR based on the field dependences of the resistance showed that its value is 1.5-2 % at room temperature.

4. CONCLUSIONS

The analysis of the experimental results concerning the structural and phase state of the thermo-, tenso- and magnetoresistive properties of $Ni_{80}Fe_{20}$ alloy films in the thickness range of 10-45 nm indicates the following:

– the samples in the temperature range of healing of defects have a stable phase state, which corresponds to the fcc-Ni_3Fe;

– the behavior of the temperature dependences of the resistivity in the first heating cycle and the value of the defect healing temperature depend on the sample thickness (a gradual increase in the defect healing temperature occurs with increasing *d*);

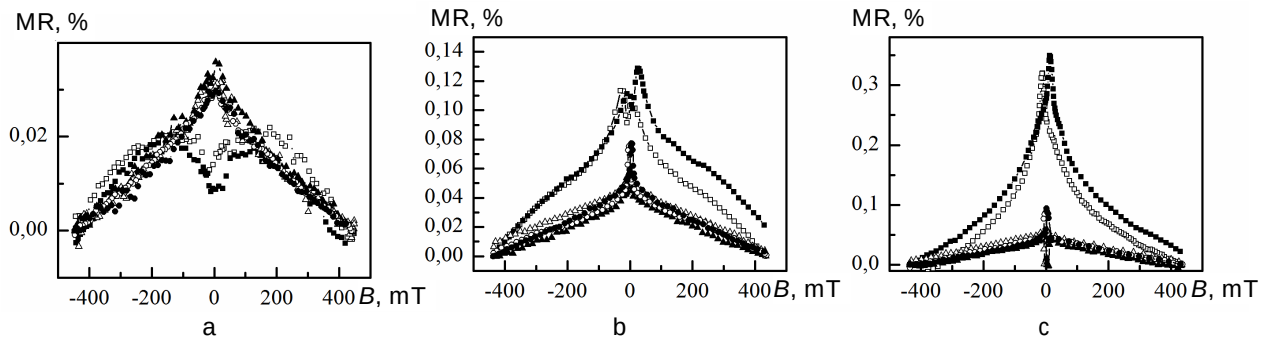

Fig. 6 – Dependence of the MR on the magnetic field induction for the $Ni_{80}Fe_{20}$(13)/Sub (a, b) and $Ni_{80}Fe_{20}$(22)/Sub films after condensation (a) and thermal annealing to T_{ann} = 470 K (b, c). The magnetic field orientation with respect to the current direction: perpendicular (□■), transverse (○●) and longitudinal (△▲)

– the size dependence of the SC differs from the classical dependence, since a gradual increase in the integral SC occurs with increasing thickness;

– the field dependences of the MR are characterized by anisotropy in the transition to the perpendicular magnetic field orientation relative to the current direction and a small value of the coercive force in the transverse and longitudinal geometries that is typical for soft magnetic materials, to which permalloy belongs.

ACKNOWLEDGEMENTS

This work has been performed under financial support of the Ministry of Education and Science of Ukraine (Grant No 0116U002623).

REFERENCES

1. Tsann Lin, Daniele Mauri, Philip M. Rice, *J. Magn. Magn. Mater.* 262, 346 (2003).
2. H. Kubota, T. Watabe, T. Miyazaki, *J. Magn. Magn. Mater.* 198-199, 173 (1999).
3. Q.H. Lu, R. Huang, L.S. Wang, Z.G. Wu, C. Li, Q. Luo, S.Y. Zuo, J. Li, D.L. Peng, G.L. Han, P.X. Yan, *J. Magn. Magn. Mater.* 394, 253 (2015).
4. Shuyun Wang, Tiejun Gao, Cuntao Wang, Jianfang He, *J. Alloy. Compd.* 554, 405 (2013).
5. Yuan-Tsung Chen, Jiun-Yi Tseng, Tzer-Shin Sheu, Y.C. Lin, S.H. Lin, *Thin Solid Films* 544, 602 (2013).
6. Gesche Nahrwold, Jan M. Scholtyssek, Sandra Motl-Ziegler, Ole Albrecht, Ulrich Merkt and Guido Meier, *J. Appl. Phys.* 108, 013907 (2010).
7. Yuan-Tsung Chen, Chia-Wen Wu, *Intermetallics* 34, 89 (2013).
8. K.V. Tyschenko, I.Yu. Protsenko, *Metallofiz. Noveishie Tekhnol.* 34 No 7, 907 (2012).
9. W. Gasior, Z. Moser, A. Debski, *J. Alloy. Compd.* 487, 132 (2009).
10. Yu.O. Shkurdoda, A.M. Chornous, V.B. Loboda, Yu.M. Shabelnyk, V.O. Kravchenko, L.V. Dekhtyaruk, *J. Nano- Electron. Phys.* 8 No 2, 02056 (2016).
11. T.M. Hrychanovska, I.Yu. Protsenko, A.M. Chornous, I.O. Shpetnyi, *Metallofiz. Noveishie Tekhnol.* 28, No 2, 267 (2006).
12. L.V. Odnodvorets, S.I. Protsenko, A.M. Chornous, *Elektrofizychni ta mahnitorezystyvni vlastyvosti plivkovykh materialiv v umovakh fazoutvorennya* : Monohrafiya (Za zah. red. prof. I.Yu. Protsenka), 203 s. (Sumy: SumDU: 2011).
13. Yuan-Tsung Chen, Jiun-Yi Tseng, S.H. Lin, T.S. Sheu, *J. Magn. Magn. Mater.* 360, 87 (2014).
14. Ia.M. Lytvynenko, I.M. Pazukha, V.V. Bibyk, *Vacuum* 116, 21 (2015).
15. K.V. Tyshenko, L.V. Odnodvorets, C.J. Panchal, I.Yu. Protsenko, *J. Nano- Electron. Phys.* 4 No 4, 04014 (2012).